Geometrical modeling of a two-dimensional sensor array for determining spatial position of a passive object

la Cour-Harbo, Anders

Document Version
Accepteret manuscript, peer-review version

Link to publication from Aalborg University

Geometrical Modeling of Two Dimensional Active Sensor for Determining Spatial Position of a Passive Object

Anders la Cour-Harbo, *Member, IEEE*

Abstract

This paper presents a model of an active sensor which can determine the spatial position of a passive object by illuminating the object via a small set of emitters and measure the intensity of the reflection by means of a small set of receivers. All emitters and receivers are located in the same two dimensional plane. The model is based on geometrical observations and provides a mapping of the measured reflected intensities to spatial position. The mapping is derived from intersection sets of prolate spheroids with emitters and receivers in the focal points, and it is shown that the mapping therefore has a series of interesting properties. Among these is a qualitatively description of the optimal position of emitters and receivers.

Keywords

sensor, active sensor, spatial position

I. INTRODUCTION

A FAST, robust, small, inexpensive, and non-contact sensor for determining the three dimensional position of a passive object is an interesting scientific challenge. The functionality of such a 3D sensor is also interesting from an industrial and commercial point of view. While it is relatively easy to construct a 3D sensor which is either fast or robust or small, it posses a significant challenge to combine the three properties in an inexpensive two dimensional sensor. This paper focuses on a generic method for designing such a sensor by means of a number of emitters and receivers positioned in two dimensions. The method is based on a series of geometrical observations and provides a model for the relation between the position of the object and the measurements which are made by means of the emitters and receivers.

It is not difficult to imagine at least a few applications of a inexpensive system for determining position. Nonetheless, the following list of examples are all ideas suggested to the author by a number of industrial partners; position of a listener in front a 3D loudspeaker system, position of a vehicle in a field of crops,

'shielding' of hazardous machinery, automated training of hand movements for proper palpation, peoples behaviour in front of an automatic door (should it open or not), and a 'touchless touch-screen'.

Note that this paper is a only a first step towards a fully functional 3D sensor. The author does not claim to have even remotely overcome the challenge of constructing a small and low-cost 3D sensors, but rather to have provided a valuable input to the process of designing and constructing the 3D sensor.

A. Background of Solutions

Many systems for determining attributes of passive objects by non-contact and non-evasive means have been proposed during the years. Such systems can be divided into two main categories; passive and active systems. The former is based purely on the signals emitted or accidentally reflected by the object, while the latter systems emit some signals towards the object and rely on the resulting reflections to acquire information about the object.

The signals received from the object can contain information in many different forms depending on what the signal has been subjected to prior to reception. Examples of phenomena affecting signals in transmission are: Variation in intensity, wavelength (like colour in light), there might be scattering, delay, or geometrical changes such as variation in signal path (caused for instance by multiple reflections), they might exhibit Doppler effect, phase distortion, or diffraction. How and which of these phenomena are exploited depends of course very much on the application.

The sensor presented here is an active system that depends solely on the intensity of reflected electro-magnetic signals. That means that the object is illuminated by a set of fixed emitters with the distinct purpose of measuring the intensity of the resulting reflection by means of receivers at a fixed set of positions. This produces a reflectance map which thus depends on the position of the emitters, the receivers, and the shape and type of surface material of the object. Systems based on this principle exists today, see for instance Rindfleisch [1], Horn [2], [3], Pentland [4], Saxberg [5] on 'shape from shading' and photoclinometry.

The main differences between previous solutions (of 'object sensors' based solely on reflected intensity) and the one presented here is 1) the relation between the amount of acquire data and the amount of desired information, 2) the need for uncorrelated data.

The most often used method for acquiring information about a passive object is through signal processing on images of the object. Although this seem like a natural approach it might be far from the optimal solution. This is particularly so if the desired information about an object is orientation, basic shape, position, colour, or other 'low rate' information. An image could for instance consist of 100×100 pixels in 8 bit gray level. That yields 80,000 bits, which then by signal processing has to be reduced to a few bits representing e.g. the orientation. Thus, a reduction of data by factor 1,000 or 10,000 is not unusual

when imagery is applied to the task of obtaining object information.

The second item is the issue of data correlation. In general, it is preferable in multi-pixel optical sensors to acquire uncorrelated data since this significantly simplifies the post-processing. For instance, in a regular photo great care has been taken to ensure that each pixel (or grain) represents the light intensity of the corresponding view-angle instead of being a mix of light intensities from many different directions. The consequence of mixing intensities from various direction is that neighboring pixels are correlated independently of object being photographed. This phenomena results in a blurred, out-of-focus photo.

B. Presented Solution

The sensor construction proposed here overcomes both of these challenges. The large data reduction is circumvented simply by using a small set of receivers. Obviously, some redundancy is necessary in the measurements if the sensor is expected to handle uncertainties such as noise and unknown surface properties of the object. However, it is not necessary to increase the number of receivers linearly compared to the needed redundancy, because we have the option of introducing multiple emitters, too. For instance, 8 emitter and 8 receivers produce the same information (quantitatively) as 1 emitter and 64 receivers. Emitting and receiving multiple signals in an efficient manner will not be discussed here. For examples of such methods see la Cour-Harbo and Stoustrup [6], Viterbi [7], Biglieri et al. [8], Molisch [9].

In the setup presented here the emitters and receivers are located such that all of them can 'see' the object at any position. Thus, in some sense the proposed sensor construction resembles a $m \times n$ camera with full correlation between pixels (completely out-of-focus), where m and n are the numbers of emitters and receivers. The challenge is then to extract the desire information, i.e. the position of the object by suitable algorithms. Note that it is not the intention to decorrelate the information for the purpose of making a low resolution image of the object.

The approach presented here is based on the assumption that the reflected intensities depends in a predictable way on the distance from emitter to object to receiver. Obviously, it is easy to determine the position when absolute distance measurements to the object are known, and it is therefore tempting to suggest measuring time-of-flight rather than intensity of the reflected signal.

Nonetheless, the reflection intensity is the method chosen for the 3D sensor solution presented here. This is because in many cases the hardware requirements for this solution are very modest as only a few low-cost emitter and receivers are needed besides the basic analog circuitry, and the production cost of the sensors is thus comparatively low. Obviously, a signal processor of some sort is necessary to convert reflected intensity to spatial position, but this may in many cases be significantly cheaper than the hardware required in traditional spatial position sensors (such as radar or sonic equipment).
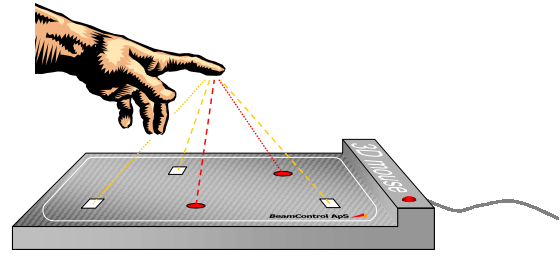
Fig. 1.   The physical design and basic principle of the 3D mouse. A number of infrared emitters (circles) and receivers (squares) are located in the 3D mouse under the infrared transparent top cover.

C. The 3D Mouse

To make the challenge more tangible it is useful to have a specific application in mind. The author suggests an infrared touch-free 3D mouse. The 3D mouse can 'read' the position of a hand (or less ambitiously, a ball on a stick). Many other positioning systems could be used, but the 3D mouse has been chosen because it is cheap and relatively easy to build (once the theory is ready to be put to a test), has suitable real time requirements, is of some commercial interest, and it has 'laboratory-friendly' dimensions.

The 3D mouse consists of a number of infrared emitters and receivers located in two dimensions, i.e. in a plane, and all are facing in the direction of the normal to the plane. The emitters emits signals from various position and the receivers measure the reflected intensities, also from a number of different positions. The relations between the intensities are then converted to a spatial position. The signals are infrared light, and the infrared emitters and receivers are located in a box with dimensions equivalent to a thick ordinary mouse pad. The physical design and basic principle of the 3D mouse is shown in Fig. 1.

II.   Determining the Spatial Position

The basic mathematical problem in determining the spatial position is mapping a high dimensional data vector, which is noisy measurements made on an object in space, into a three dimensional data vector containing the coordinates of the object. The challenge is not to define or create the mapping per se, but to devise a method that produces a fairly accurate result when noise is present in the measurements.

There are a number of a priori feasible ways for converting the measurements, ranging from purely analytical derived equations to a table of a discretized mapping based on meticulously measured reflection intensities for all object positions. The former is definitely preferable to the latter since an analytical approach (potentially) allows for parameterization of the mapping. This would be quite useful in applications where the conditions are likely to change. An analytical approach is necessarily based on some sort of modeling, and an important question is how extensive the model has to be. This is in turn dependent on

the requirements on the mapping which are imposed to ensure that it is can be used in real applications. The following prioritized list shows these requirements. The mapping

1. works well for good and accurate measurements,

2. yields a reasonable relation between error in measurements and error in 3D position,

3. has low computational complexity,

4. has low dynamic range in computations,

5. is easily adaptable in real time.

Since the measurements are expected to be good most of the time, the primary concern is that the mapping does well in this case, and the second requirement ensures that a small decrease in accuracy does not result in too large deviations in the spatial position.

In an attempt to construct a mapping by theoretical means a geometrical description is presented. Other means have been explored as well, but these are not reported here.

The mapping of high dimensional data to three dimensional position can, theoretically, be accomplished by purely geometrical consideration. This approach requires models of the individual physical components in the setup, which in turn requires a series of assumptions and approximations. The use of geometry in combination with approximations of various kinds can be challenging, because geometric equations tend to be numerically sensitive. The fact that the measurements usually originates in signals with a low SNR only makes the geometric solution even more challenging.

The assumptions used for the modeling lead to a description of the mapping by a set of equations describing intersection curves for three dimensional prolate spheroids, that is ellipses revolved around their semimajor axes. This paper presents the making of the mapping. This includes a more detailed description of the concept and assumptions leading to spheroids, a rigorous derivation of the intersection of said spheroids, and a discussion of the choice of locations of emitters and receivers.

III. Basic Concept of a Geometrical Solution

The construction starts with the observation that an emitter/receiver (E/R) pair transmits an 'amount' of light from emitter to receiver. This amount depends on various factors such as directional characteristics of the E/R pair and the position and properties of the reflecting object. This means that there is a vector function M mapping spatial position in front of the emitter/receiver pair to an intensity. When an intensity I is measured at the receiver it is immediately known that the reflecting object is located somewhere in the iso-intensity set corresponding to I of this mapping, since the iso-intensity set is the set of points in 3D which – according to the mapping – yields a reflected intensity I. When sufficiently many such 3D sets (each set comes from a particular E/R pair) are known for the same object, the intersection of these sets is a single point, which is then the location of the object. What we want eventually is the 'reverse'

mapping $\mathcal{I}$, called the intersection function, which given a set of intensities (that is the measurements) provides the intersection point for the iso-intensity sets corresponding to those intensities, thus yielding the spatial position of the reflecting object.

The reflecting object is assumed to have properties (see the next section) such that this mapping $M : \mathbb{R}^3 \mapsto \mathbb{R}$ is on the form

$$M(\mathbf{p}) = \left(\|\mathbf{p} - \mathbf{e}\| + \|\mathbf{p} - \mathbf{r}\| \right)^{-2} , \tag{1}$$

where $\mathbf{p}$, $\mathbf{e}$, and $\mathbf{r}$ are the spatial positions of the object, the emitter, and the receiver, respectively, and $\| \cdot \|$ is the Euclidean norm. The locus of $M(\mathbf{p}) = $ constant is easily seen to be a prolate spheroid with focal points in $\mathbf{e}$ and $\mathbf{r}$. Note that this particular observation is independent of the power -2, which is included here to model the reduction of the intensity by the square of the distance to the object.

The $+$ sign in (1) holds the implicit assumption of a specular reflection in the direction of the receiver, i.e. that the light 'continues on' to the receiver when reflected instead of being scattered or reflected in another direction. If the object has a completely diffuse reflection function would be along the lines of the form

$$M(\mathbf{p}) = \left(\|\mathbf{p} - \mathbf{e}\| \|\mathbf{p} - \mathbf{r}\| \right)^{-2} , \tag{2}$$

that is with multiplication rather than addition. The reflection map is somewhat different from that of (1). The form (2) is admittedly strongly simplified, but it does show the basic form when two 'scatterings' are involved (the first 'scattering' as the emitter emits light in many directions).

IV. ASSUMPTIONS

Obviously, in any application the mapping M also depends on the orientation and reflectivity of the object, and the characteristics of the emitters and receivers. In this presentation these unknowns have been assumed to be relatively simple. The object is assumed to be homogeneous and rotational invariant (a disc in 2D, a ball in 3D). That is, the reflection is independent of the orientation of the object. Also, the emitter and receiver characteristics are assumed to be uniform. It is important to note that the idea of analytically deriving the intersection function for the iso-intensity sets does not depend in a fundamental way on the aforementioned properties (the complexity of the approach does to a very high degree, though). Consequently, the assumptions are chosen such that they are very simple and results in a relatively simple intersection function $\mathcal{I}$.

Since it is a priori unknown what the optimal locations of emitters and receivers are it is desirable to have complete freedom. The question of the optimal locations of E/Rs is discussed in Section IX. In this model there is only one requirement. The emitters and receivers have to be located such that each emitter is located adjacent to a receiver. Such an E/R pair is in this paper referred to as a sensor. Note that it still

makes sense to talk about an E/R pair, which is an emitter and a receiver that are not necessarily adjacent.

The ever present problem of noise has not been directly accounted for in this model. This means that there has been no attempt to robustify the equations (for instance by adding some kind of low pass filtering property). There is a priori no guarantee that even small perturbations of the high dimensional data will be handled properly. However, simulations show that the mapping behaves quite nicely. Further, one analytical step has been taken to reduce the influence of noise. This is related to the location of the sensors.

Finally, a comment on the assumption on the shape and surface of the reflection object. As mentioned above the modeling is based on (1), i.e. that the surface has a specular reflection in the direction of the receiver (a reduction of the intensity is allowed). This can be achieved by a plane mirror positioned such that it is tangent to the spheroid with focal points in the emitter and the receiver, or by a spherical mirror. At the same time the reflection has to occur at the same point in 3D for all involved pairs of E/Rs (to justify the idea of a spheroids intersection point). The obvious conflict in 'the spheroid assumption' (that is, having reflection in different direction at the same point) is a potential problem in real applications. However, a possible solution (or rather a compromise between conflicting interests) is discussed in Section X.

Note that the albedo of the object is accounted for in the model, since it includes a uniform scaling of all the intensity measurements.

The advantage of modeling the 3D sensor by means of spheroids is the existence of a relatively simple analytical description of the mapping from high dimensional measurement data to a spatial position. This is the subject of the following section. Note that the mapping is constructed in a completely mathematical setting in the sense that no further physical assumptions are introduced. Consequently, the model is generic rather than explicit, and a discussion of issues such as choice of materials, power consumption, response time, physical units, and the like is not relevant here. This does not mean that such matters are of no importance, but they are related to particular embodiments of the 3D sensor rather than the development of the generic model.

V. The Intersection Function

The smallest number of spheroids with which it is possible to uniquely determine an intersection point is three. The smallest number of sensors that gives three spheroid is also three. From this set of three sensors any two give the focal points of a spheroid. The objective of this section is to construct the function which maps these three spheroids with different semimajor axes given by the three measured intensities into that particular point in 3D where they intersect. The measured intensities are not used 'as is' since the transmitted light is subjected to a unknown reduction (governed by the reflectivity of the object and

amplification in the receiver) and since the there is a $(\cdot)^{-2}$ relation between measured intensities and relative distances. This is explained in later in this section. To account for this the intensities are all subjected to $(\cdot)^{-2}$ and scaled by a common factor r. Note also that the focal points are always in the xy plane.

A. Definitions

Before deriving the intersection function it is convenient to reduce the number of degrees of freedom to a minimum by means of scaling, rotation, and translation of the triangles spanned by the sensors. In order to do this a few new variables are needed.

Definition 1 (Focal Points) Let P, Q, and S be three points in the xy plane. Define the vectors

$$\mathbf{p} = \begin{bmatrix} Q_1 - S_1 \\ Q_2 - S_2 \end{bmatrix}, \quad \mathbf{q} = \begin{bmatrix} P_1 - S_1 \\ P_2 - S_2 \end{bmatrix}, \quad \mathbf{s} = \begin{bmatrix} Q_1 - P_1 \\ Q_2 - P_2 \end{bmatrix},$$

define the angle

$$\theta = \frac{q_2}{|q_2|} \arccos\left(\frac{q_1}{\|\mathbf{q}\|}\right),$$

and define $\mathbf{d}$ and γ as

$$\mathbf{G}(\theta) \begin{bmatrix} \mathbf{q} & \mathbf{p} \\ 0 & 0 \end{bmatrix} = 2\gamma \begin{bmatrix} d_1 & d_2 \\ 0 & 1 \\ 0 & 0 \end{bmatrix},$$

where

$$\mathbf{G}(\theta) = \begin{bmatrix} \cos\theta & \sin\theta & 0 \\ -\sin\theta & \cos\theta & 0 \\ 0 & 0 & 1 \end{bmatrix}$$

is a clockwise rotation θ radians of a point in $\mathbb{R}^3$ around the z axis. The points PQS must be such that

$$(\mathbf{s} \times \mathbf{q})^\top \begin{bmatrix} 0 \\ 0 \\ 1 \end{bmatrix} > 0 \quad \text{and} \quad \mathbf{p}^\top \mathbf{q} < \|\mathbf{p}\|\|\mathbf{q}\|,$$

and $d_1 \geq d_2 \geq 0$.

The definition is closely related to Fig. 2.

Note that any set of three points in the xy plane complies with this definition when

1. they are not lying on a line,

2. they are enumerate with P, Q, and S counter-clockwise

3. Q is associated with the obtuse angle (whenever there is one).

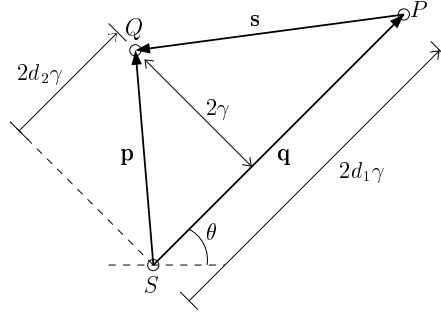Thus, effectively, this includes all triangles.

Fig. 2. The setup for the focal points.

The next step is to introduce the spheroids. According to the assumptions they are prolate spheroids, that is they are given as the loci of revolutions of ellipses around their semimajor axes. Any prolate spheroid with focal points in the xy plane is generated by revolving an ellipse

$$\frac{(x - x_0)^2}{r_1^2} + \frac{(y - y_0)^2}{r_2^2} = 1 \tag{3}$$

with centre (x_0, y_0) around the line $\begin{bmatrix} x_0 + t & y_0 & 0 \end{bmatrix}$ followed by a rotation θ clockwise around the line $\begin{bmatrix} x_0 & y_0 & t \end{bmatrix}$. Such a spheroid can also be defined by a single expression. Define the prolate spheroid form $E : \mathbb{R}^3 \otimes \mathbb{R}^2 \otimes \mathbb{R} \mapsto \mathbb{R}$ as

$$E(\mathbf{c}, \mathbf{r}, \theta) = \mathbf{c}^\top \mathbf{G}(\theta) \begin{bmatrix} r_1 & 0 & 0 \\ 0 & r_2 & 0 \\ 0 & 0 & r_2 \end{bmatrix}^{-1} \mathbf{G}(-\theta)\mathbf{c}.$$

Then the locus of

$$E\left(\begin{bmatrix} x - x_0 \\ y - y_0 \\ z \end{bmatrix}, \begin{bmatrix} r_1^2 \\ r_2^2 \end{bmatrix}, \theta \right) = 1 . \tag{4}$$

is a prolate spheroid with centre in (x_0, y_0) and with the semimajor axis in an angle of $-\theta$ to the x axis. This is easily seen. Assume for simplicity that $x_0 = y_0 = 0$. Expanding (4) then yields

$$\frac{(x \cos\theta - y \sin\theta)^2}{r_1^2} + \frac{(x \sin\theta + y \cos\theta)^2}{r_2^2} + \frac{z^2}{r_2^2} = 1. \tag{5}$$

Define the result of a counter-clockwise rotation of the locus of (5) around the z axis as $\begin{bmatrix} \tilde{x} & \tilde{y} & 0 \end{bmatrix}^\top = \mathbf{G}(-\theta) \begin{bmatrix} x & y & 0 \end{bmatrix}^\top$. Then

$$\frac{\tilde{x}^2}{r_1^2} + \frac{\tilde{y}^2}{r_2^2} + \frac{z^2}{r_2^2} = 1,$$
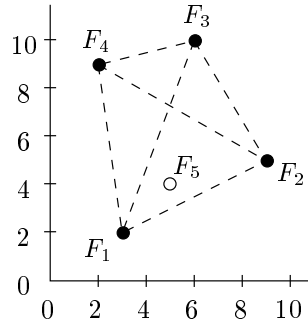
Fig. 3. The locations of the four sensors and the projection onto the xy plane of the location of the object.

TABLE I

THE VALUES ACCORDING TO DEFINITION 1 FOR THE FOUR TRIANGLE.

Triangle	θ	γ	d_1	d_2
$F_1F_2F_3$	$\arccos\left(\frac{3}{\sqrt{73}}\right) - \pi$ -1.9296	$\frac{39}{2\sqrt{73}}$ 2.2823	$\frac{73}{39}$ 1.8718	$\frac{31}{39}$ 0.79487
$F_2F_3F_4$	$-\arccos\left(\frac{7}{\sqrt{65}}\right)$ -0.51915	$\frac{23}{2\sqrt{65}}$ 1.4264	$\frac{65}{23}$ 2.82608	$\frac{3}{4}$ 0.75000
$F_3F_4F_1$	$\arccos\left(\frac{3}{\sqrt{73}}\right)$ 1.2120	$\frac{29}{2\sqrt{73}}$ 1.6971	$\frac{73}{29}$ 2.5172	$\frac{53}{29}$ 1.8276
$F_4F_1F_2$	$\pi - \arccos\left(\frac{7}{\sqrt{65}}\right)$ 2.6224	$\frac{45}{2\sqrt{65}}$ 2.7908	$\frac{13}{9}$ 1.4444	$\frac{2}{3}$ 0.66667

which is the result of revolving the ellipse (3) around the x axis.

Finally, the positive orthant is referred to several times in the following.

Notation 2: The positive orthant of $\mathbb{R}^N$ is that subset of $\mathbb{R}^N$ for which all coordinates are ≥ 0. This subset is denoted $\mathbb{R}^{N+}$. For $N = 1$ the notation $\mathbb{R}^+$ is used.

B. Examples

Throughout this presentation a number of examples will be given to support the theoretical derivations. The examples are all based on the same setup which is presented here.

A total of four sensors are located in the xy plane at $F_1 : (3, 2)$, $F_2 : (9, 5)$, $F_3 : (6, 10)$, and $F_4 : (2, 9)$, see Fig. 3. This generates four triangles $F_1F_2F_3$, $F_2F_3F_4$, $F_3F_4F_1$, and $F_4F_1F_2$ (which all complies with Definition 1). The reflecting object is located in $F_5 : (5, 4, 3)$. This point gives a set of measurements which are related to the distances from the sensors to the point (i.e. the object). While measured reflected

Sensor pair	Measurement
$F_1 F_2$	9.2221
$F_1 F_3$	10.905
$F_1 F_4$	10.681
$F_2 F_3$	11.881
$F_2 F_4$	11.656
$F_3 F_4$	13.340

intensities are proportional to the square of reciprocal of the distance, the 'measurements' used in the following equations are assumed to be proportional to the distance. Thus, in a real application it is necessary to apply a mapping on the form $(\cdot)^{-2}$ to the measured intensities. Note that the mapped measurements are also referred to as measurements.

There are two equal measurements for each sensor pair. In a real setup the two measurements will most likely not be equal due to noise, and the redundancy can then be used to decrease the noise level. Since there are a total of six different combinations of two sensors there are also six measurements. Simulated measurements corresponding to the point F_5 are given in Table II. Here the measurements are actually the sum of the distance from the object to the two sensors, and not intensities.

C. Fixing the Focal Points

The general intersection function which will be derived in Section VI is based on an intersection function for spheroids with fixed focal points. Actually, the section title is slightly misleading since they are not all fixed, but the restrictions imposed on them reduce the number of degrees of freedom from six (three points times two dimension) to three. This simplifies the construction somewhat and the remaining degrees of freedom are easily introduced again later.

Since each set of three spheroids will generate exactly one intersection function the following derivations are, unless otherwise stated, for three spheroids and their three focal points.

The three focal points are denoted P, Q, and S (see also Fig. 2). The point S is fixed in the origin $(0, 0)$, the point P is constrained to the x axis, that is $P = (2d_1, 0)$ with $d_1 > 0$, and Q is constrained to the horizontal line $x = 2$, i.e. $Q = (2d_2, 2)$. Furthermore, Q is always the obtuse angle, so we also have $0 \leq d_2 \leq d_1$. This is equivalent to Definition 1 with $\theta = 0$ and $\gamma = 1$. To avoid symmetry one more restriction could be imposed (for instance $2d_2 < d_1$). However, this 'redundancy' does not complicate

the following computations (they are actually a little easier without this restriction), and moreover, it does not reduce the number of degrees of freedom.

The three spheroids generated by the three focal points each have one degree of freedom, namely one of their semi axes. In this setup the semimajor axes are free. The measurements made in the physical setup are the intensities of the reflected and received light. The results of the $(\cdot)^{-2}$ conversion are denoted w_1, w_2, and w_3, and corresponds to the measurements made for PQ, QS, and PS pairs, respectively. That is, a w_k is proportional to the distance from an emitter to the object plus the distance from the object to a receiver. The assumption that all emitters have the same uniform characteristics (and ditto for the receivers) leads to a single unknown variable r, which represents the level or amplitude of these characteristics.

In the following equations describing the three spheroids with focal points in PQ, QS and PS, respectively, the semimajor axes are $w_n r$, and the semiminor axes are computed based on the fact that the square of the semimajor axis equals the square of the distance between focal points minus the square of the semiminor axis.

$$PQ: \quad E\left(\begin{bmatrix} x - d_1 - d_2 \\ y - 1 \\ z \end{bmatrix}, \begin{bmatrix} w_1^2 r^2 \\ w_1^2 r^2 - (d_1 - d_2)^2 - 1 \end{bmatrix}, \arctan\left((d_1 - d_2)^{-1}\right) \right) = 1 \qquad (6)$$

$$QS: \quad E\left(\begin{bmatrix} x - d_2 \\ y - 1 \\ z \end{bmatrix}, \begin{bmatrix} w_2^2 r^2 \\ w_2^2 r^2 - d_2^2 - 1 \end{bmatrix}, -\arctan d_2^{-1} \right) = 1 \qquad (7)$$

$$PS: \quad E\left(\begin{bmatrix} x - d_1 \\ y \\ z \end{bmatrix}, \begin{bmatrix} w_3^2 r^2 \\ w_3^2 r^2 - d_1^2 \end{bmatrix}, 0 \right) = 1 \qquad (8)$$

All the expressions in the above equations are easily derived from geometrical observations using the triangle in Fig. 2.

The purpose of this Section V is to demonstrate that for all values fixed such three spheroids have at most one intersection point in $\mathbb{R}^2 \otimes \mathbb{R}^+$, and that the locus of the intersection for variable r is a well-defined and well-behaved curve. Further, it is demonstrated that the same holds for the more general case with arbitrary focal points. This is done in several steps, starting in the next subsection with an exemplification of the restriction introduced previously. This is followed by the derivation of the intersection function in the restricted case. Finally, the general case is treated.

D. One Embodiment of the Spheroids

Assume that a reflecting object has been positioned in F_5 and that the measurements given in Table II have been obtained. Using (6) through (8) three spheroids can be constructed, each corresponding to a set of two corners in, say, the triangle $F_3 F_4 F_1$. The Fig. 4 shows the triangle $F_3 F_4 F_1$ subjected to the restrictions described above (and thus renamed PQS), and z contours of the corresponding spheroids for fixed $r = 0.295 = 1/(2\gamma)$. The third row in Table I gives the scaling and rotation necessary to map between $F_3 F_4 F_1$ and PQS. The point F_5 is relocated by the scaling, rotation and translation from $(5, 4, 3)$ to $(1.52, -0.690, 1.77)$, approximately. This point is denoted F_5'. Since all the points have shifted, the distances between the corners of the triangle and F_5' have changed, too. Consequently, the values in Table II do not equal the distances in the PQS setup. However, the scaling (which is the only operation that matters in this context) scales the distances equally, and since the scaling is known the (simulated) measurements can be converted to match the PQS setup by division by γ. Note, however, that this division is not necessary in relation to the intersection function presented shortly since the r factor in the spheroid equations also scales the measurements equally. The measurements needed in the present triangle is $w_1 = F_3 F_4$, $w_2 = F_1 F_4$, and $w_3 = F_1 F_3$ from Table II.

In Fig. 4 the contours of the three spheroids with $r = 0.295$ are shown for $z = 0$ and $z = 1.77$. Note how the contours all meet in F_5' for the latter choice of z. In the following sections the relation between $\mathbf{w}$, the (x, y, z) coordinate of the intersection, and r is given. For instance, it will be evident that for a given admissible choice of $\mathbf{w}$ (meaning that it comes from a point in 3D) there is a unique vector function $\mathcal{I} : \mathbb{R}^+ \mapsto \mathbb{R}^2 \otimes \mathbb{R}^+$ mapping r to a space curve such that the correct 3D point (the one which corresponds to $\mathbf{w}$) is the result of the mapping exactly when $r = 1/(2\gamma)$.

It is important to note that in a real setup the 'admissible measurements' are known up to a scaling factor, which means that it is not $\mathbf{w}$, but rather $a\mathbf{w}$ for some unknown a that fits the description in the previous paragraph. Thus, knowing γ is not sufficient information to determine the correct point in 3D. The r factor has been introduced for the very purpose of accommodating this particular 'lack of information'.

E. Intersection for Fixed Focal Points

The intersection function for the restricted setup is presented in this section. The function is derived on the basis of purely geometrical considerations, namely by solving the three spheroid equations simultaneously.

In the following we will need quantities on the form $w_n - w_k$ several times. The notation w_{nk} will be used as an 'acronym' for this.
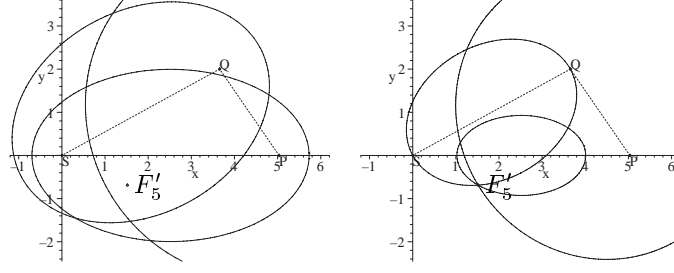
Fig. 4. The triangle PQS is $F_3F_4F_1$ scaled, rotated, and shifted according to Table I. The left plot shows the contour of the corresponding spheroids for $z = 0$, and the right plot shows the contour of the spheroids for $z = 1.77$. In both plots $r = 0.295$. The values in Table I and II have been used.

Lemma 3: The (x, y, z) solution to the set of equations (6), (7), and (8) for which $z \geq 0$ when $\mathbf{w}$ corresponds to a point in (x, y, z) space is a vector function $\mathbb{R}^{6+} \mapsto \mathbb{R}^2 \otimes \mathbb{C}$ given by

$$\widetilde{\mathcal{I}}^\triangle(\mathbf{w}, \mathbf{d}, r) = \begin{bmatrix} x \\ y \\ z \end{bmatrix} = \frac{1}{d_1} \begin{bmatrix} w_{21}w_3 r^2 + d_1^2 \\ (d_1 w_2 w_{31} + d_2 w_3 w_{12})r^2 + d_1(1 - d_1 d_2 + d_2^2) \\ \sqrt{A^\triangle(\mathbf{w}, \mathbf{d})r^4 + B^\triangle(\mathbf{w}, \mathbf{d})r^2 + C^\triangle(\mathbf{d})} \end{bmatrix}, \qquad (9)$$

where

$$A^\triangle(\mathbf{w}, \mathbf{d}) = -\left[d_2 w_{12} w_3 - d_1 w_{13} w_2\right]^2 - w_{12}^2 w_3^2$$

$$B^\triangle(\mathbf{w}, \mathbf{d}) = 2d_1 d_2 w_3 w_{12}(d_1 d_2 - d_2^2 - 1) + d_1^2\left(w_{23}^2 + 2d_2 w_2 w_{13}(d_2 - d_1) + w_1^2\right)$$

$$C^\triangle(\mathbf{d}) = -d_1^2(d_2^2 + 1)((d_1 - d_2)^2 + 1) .$$

The notation $\widetilde{\mathcal{I}}^\triangle(r)$ is used when $\mathbf{w}$ and $\mathbf{d}$ are fixed.

Proof: A proper scaling of (8) followed by a subtraction of (8) from (7) eliminates z, and a second degree equation in x emerges. (The trigonometric functions resolve nicely). The two solutions to this equation are then inserted in (6) and (8). Another scaling followed by a subtraction yields two other second degree polynomials in y, which then gives four candidates for y. Inserting those along with the corresponding x in (7) gives a total of eight candidates for z, all on this $\pm\sqrt{\cdot}$ form. Since we are interested in $z \geq 0$, we are left with four z candidates. The true solution is found by choosing a point in space and three focal points, determine the corresponding $\mathbf{w}$, $\mathbf{d}$, and r, inserting this set of arguments into z. Only one candidate will then yield a real z coordinate. This z and the corresponding x and y are given in (9). ∎

It is obvious from (9) that the x and y coordinates will be real independently of the choice of $\mathbf{w}$ and $\mathbf{d}$. This is not the case for z, however. Because on the one hand a choice of $\mathbf{w}$ which makes the spheroids too small or too large to intersect cannot give a real z for any r, and on the other hand choosing $\mathbf{w}$ such that

it matches a particular point in $\mathbb{R}^2 \otimes \mathbb{R}^+$ must give a real z for some r. Based on this, and the previous observations, and a continuity argument we can conclude the following:

Lemma 4: The z in $\widetilde{\mathcal{I}}^\triangle(\mathbf{w}, \mathbf{d}, r)$ in Lemma 3 is real iff there exists $t \in \mathbb{R}^+$ such that $\widetilde{\mathcal{I}}^\triangle(t\mathbf{w}, \mathbf{d}, r) \in \mathbb{R}^2 \otimes \mathbb{R}^+$ and r belongs to an interval on the form

$$[\frac{t}{2\gamma} - e_1; \frac{t}{2\gamma} + e_2] \subset \mathbb{R}^+$$

where $e_1, e_2 > 0$.

Note that $\widetilde{\mathcal{I}}^\triangle$ was constructed under the assumption that $\gamma = 1$, and the lemma therefore currently applies only in this case. However, later it will be evident that this restriction have no influence on the observations that lead to this lemma, and consequently the lemma also holds in the general case presented in Section VI.

Based on the lemma it is easy to give a definition of admissible measurements; it is exactly those points $\mathbf{w} \in \mathbb{R}^{3+}$ which corresponds to a point (x, y, z) in $\mathbb{R}^2 \otimes \mathbb{R}^+$, as stated in the lemma.

Definition 5: Let P, Q, and S be three points satisfying definition 1. The set $\mathcal{F}^\triangle_{PQS}$ is defined as the set of vectors $\mathbf{u} \in \mathbb{R}^{3+}$ for which there exist a point $P_0 = (x, y, z) \in \mathbb{R}^2 \otimes \mathbb{R}^+$ and $r > 0$ such that

$$ru_1 = \text{dist}(P_0, P) + \text{dist}(P_0, Q),$$
$$ru_2 = \text{dist}(P_0, Q) + \text{dist}(P_0, S),$$
$$ru_3 = \text{dist}(P_0, P) + \text{dist}(P_0, S).$$

The same observations made for intersections of the spheroids can be made for intersection of the spheres. It is therefore relevant to have the following definition.

Definition 6: Let P, Q, and S be three points satisfying definition 1. The set $\mathcal{F}^\circ_{PQS}$ is defined as the set of vectors $\mathbf{u} \in \mathbb{R}^{3+}$ for which there exist a point $P_0 = (x, y, z) \in \mathbb{R}^2 \otimes \mathbb{R}^+$ and $r > 0$ such that

$$ru_1 = 2 \cdot \text{dist}(P_0, P),$$
$$ru_2 = 2 \cdot \text{dist}(P_0, Q),$$
$$ru_3 = 2 \cdot \text{dist}(P_0, S).$$

The factor 2 is included to ensure that r in the two definitions have the interpretation.

We are now finally ready to state the unified result for the intersection set of the spheroids.

Theorem 7: The three spheroids (6), (7), and (8) intersect iff $r\mathbf{w} \in \mathcal{F}^\triangle_{PQS}$. In this case the particular intersection function $\widetilde{\mathcal{I}}^\triangle(r)$ is mapping $I \subset \mathbb{R}^+$ into $\mathbb{R}^2 \otimes \mathbb{R}^+$, where I is a compact set. The intersection point of the spheroids is given by $\widetilde{\mathcal{I}}^\triangle(r_0)$ for some $r_0 \in I$.

Since it is assumed that there is a sensor at each focal point, there will also be measurements available for the reflected intensity of light emitted from and received at the same point (the same sensor).
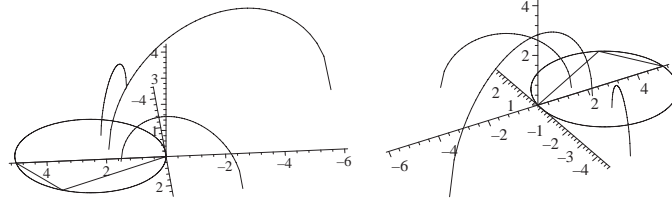
Fig. 5. Three intersection curves generated by $\widetilde{\mathcal{I}}^{\triangle}(\mathbf{w}, \mathbf{d}, r)$ with values from Table I and II. The two plots show the same curves from two different view angles. The three curves (clockwise seen from the center of the circle) have w_2 modified by -1.5, 0, and 1.2. The intervals for r are $[0.275; 0.560]$, $[0.236; 0.854]$, and $[0.233; 2.14]$, respectively. Note that they all include $1/(2\gamma) = 0.295$. The circumscribed circle to the PQS triangle is also shown in the xy plane.

Theorem 8: The exists a solution $(x, y, z) \in \mathbb{R}^2 \otimes \mathbb{R}^+$ to the following set of spheres equations

$$P : \qquad (x - 2d_1)^2 + y^2 + z^2 = v_1^2 r^2 \qquad (10)$$

$$Q : \qquad (x - 2d_2)^2 + (y - 2)^2 + z^2 = v_2^2 r^2 \qquad (11)$$

$$S : \qquad x^2 + y^2 + z^2 = v_3^2 r^2 \qquad (12)$$

iff $r\mathbf{v} \in \mathcal{F}_{PQS}^\circ$, and this solution is given by

$$\widetilde{\mathcal{I}}^\circ(\mathbf{v}, \mathbf{d}, r) = \frac{1}{4d_1} \begin{bmatrix} (v_3^2 - v_1^2)r^2 + 4d_1^2 \\ (d_1(v_3^2 - v_2^2) - d_2(v_3^2 - v_1^2))r^2 + 4d_1(1 - d_1d_2 + d_2^2) \\ \sqrt{A^\circ(\mathbf{w}, \mathbf{d})r^4 + B^\circ(\mathbf{w}, \mathbf{d})r^2 + C^\circ(\mathbf{d})} \end{bmatrix} \qquad (13)$$

where

$$A^\circ(\mathbf{v}, \mathbf{d}) = -\left(d_1(v_2^2 - v_3^2) + d_2(v_3^2 - v_1^2)\right)^2 - (v_1^2 - v_3^2)^2$$

$$B^\circ(\mathbf{v}, \mathbf{d}) = 8d_1\left(d_1(d_2(d_2 - d_1) + 1)v_2^2\right.$$
$$\left. + d_2((d_1 - d_2)^2 + 1)v_3^2 + (d_1 - d_2)(d_2^2 + 1)v_1^2\right)$$

$$C^\circ(\mathbf{d}) = -16d_1^2(d_2^2 + 1)\left((d_1 - d_2)^2 + 1\right).$$

In this case $\widetilde{\mathcal{I}}^\circ(r)$ is mapping $I \subset \mathbb{R}^+$ into $\mathbb{R}^2 \otimes \mathbb{R}^+$, where I is a compact set. The intersection point of the spheroids is given by $\widetilde{\mathcal{I}}^\circ(r_0)$ for some $r_0 \in I$.

To illustrate the result of applying $\widetilde{\mathcal{I}}^{\triangle}(r)$ to an actual case Fig. 5 shows three intersection sets. They appear to be well-behaved, and it is demonstrated in the next section that this is actually always the case for intersection sets of spheroids and spheres (under the given assumptions and constraints presented previously).

VI. The General Intersection Function

Having introduced the particular intersection functions which are valid only for sensors located at rather restricted locations in the xy plane, we are now ready to relax some of these conditions. This is done by returning to the original definition of sensor locations, that is Definition 1. To extend the intersection function presented in the previous section all that is necessary is to perform the inverse of the scaling, rotation, and translation which was applied to the general case in order to restrict it to the particular case.

At the same time the variables γ, θ, d_1, and d_2 are 'hidden' in the general intersection function since they relate, in a sense, to the particular case, whereas the PQS notation is more natural in the general case. A new and more simple definition of the intersecting objects is therefore also given. It is based on the immediately available information, that is the sensor locations, rather than the derived quantities θ, γ, d_1, and d_2.

Definition 9 (Prolate Spheriod II) Let $\mathcal{E}(H, G, a)$ denote the locus of a prolate spheroid constructed by revolving an ellipse with focal points in H and G around the semimajor axis a.

Note that $\mathcal{E}(H, H, a)$ will give a sphere with centre in H and radius a.

This definition allows a simple formulation of the general intersection functions.

Theorem 10 (The Intersection Functions) Let P, Q, and S be three points satisfying definition 1. The three spheroids $\mathcal{E}(P, Q, w_1 r)$, $\mathcal{E}(Q, S, w_2 r)$, and $\mathcal{E}(P, S, w_3 r)$ intersect iff $r\mathbf{w} \in \mathcal{F}^{\triangle}_{PQS}$. The intersection point is given by

$$\mathcal{I}^{\triangle}_{PQS}(\mathbf{w}, r) = \gamma \mathbf{G}(-\theta) \widetilde{\mathcal{I}}^{\triangle}(\mathbf{w}, \mathbf{d}, r) + [S_1 \ S_2 \ 0]^{\top}. \tag{14}$$

Equivalently, the three spheres $\mathcal{E}(P, P, v_1 r)$, $\mathcal{E}(Q, Q, v_2 r)$, and $\mathcal{E}(S, S, v_3 r)$ intersect iff $r\mathbf{v} \in \mathcal{F}^{\circ}_{PQS}$. The intersection point is given by

$$\mathcal{I}^{\circ}_{PQS}(\mathbf{v}, r) = \gamma \mathbf{G}(-\theta) \widetilde{\mathcal{I}}^{\circ}(\mathbf{v}, \mathbf{d}, r) + [S_1 \ S_2 \ 0]^{\top}. \tag{15}$$

The functions $\mathcal{I}^{\triangle}_{PQS}(\mathbf{w}, r)$ and $\mathcal{I}^{\circ}_{PQS}(\mathbf{v}, r)$ are undefined when $r\mathbf{w} \notin \mathcal{F}^{\triangle}_{PQS}$ and $r\mathbf{v} \notin \mathcal{F}^{\circ}_{PQS}$, respectively.

It was stated earlier that the intersection set generated by a varying r and fixed $\mathbf{w}$ produced a well-behaved curve. This was also demonstrated for a few examples of $\mathbf{w}$ in Fig. 5. The following lemma shows that this is indeed always the case, and, moreover, that this set is always a half circle.

Lemma 11: Let P, Q, and S be three points satisfying Definition 1, and let $\mathbf{w} \in \mathcal{F}^{\triangle}_{PQS}$. Then $\mathcal{I}^{\triangle}_{PQS}(r)$ equals the intersection of $\mathbb{R}^2 \otimes \mathbb{R}^+$ and a circle with centre in the xy plane. The projection of this circle onto the xy plane is part of a line which goes through the center of the circumscribed circle to the triangle PQS. This also holds for $\mathcal{I}^{\circ}_{PQS}(r)$ with $\mathbf{v} \in \mathcal{F}^{\circ}_{PQS}$.
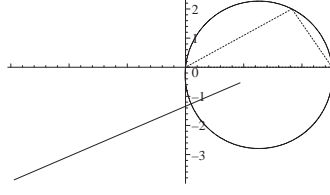
Fig. 6. The projection onto the xy plane of an intersection set is part of a line which goes through the centre of the circumscribed circle. Here this is exemplified for $F_3 F_4 F_1$ using values from Table I and Table II are used. The line is the projection of the larger curve in Fig. 5 on to the xy plane.

The projection on the xy plane of an intersection set is shown in Fig. 6.

Proof: The projection of $\widetilde{\mathcal{I}}^\triangle$ onto the xy plane is

$$\begin{bmatrix} x \\ y \end{bmatrix} = \frac{1}{d_1} \begin{bmatrix} w_{21} w_3 \\ d_1 w_2 w_{31} + d_2 w_3 w_{12} \end{bmatrix} r^2 + \begin{bmatrix} d_1 \\ 1 - d_1 d_2 + d_2^2 \end{bmatrix}. \tag{16}$$

For any fixed choice of $\mathbf{w}$ and $\mathbf{d}$ (16) is a straight line through $[d_1, \ 1 - d_1 d_2 + d_2^2]$. The center of the circumscribed circle is the intersection of the perpendicular bisectors. Two of these are given by

$$QS: \ y = -d_2 x + d_2^2 + 1, \qquad PS: \ x = d_1,$$

and the intersection of these is the point $(d_1, \ 1 - d_1 d_2 + d_2^2)$. Showing that $\widetilde{\mathcal{I}}^\triangle$ describes a circle is done in two steps. First $\widetilde{\mathcal{I}}^\triangle$ is rotated around the z axis such that the y coordinate becomes independent of r, then the xz coordinates are shown to describe a plane circle.

The angle between the line (16) and the x axis is

$$\theta = \arctan\left(\frac{d_1 w_2 w_{31} + d_2 w_3 w_{12}}{w_{21} w_3} \right).$$

By applying $\mathbf{G}(\theta)$ to $\widetilde{\mathcal{I}}^\triangle$, the x and y coordinates becomes two large expressions, where the y coordinate is independent of r. Isolating r in the x coordinate and inserting into the z coordinate yields

$$z^2 = -x^2 + \frac{p_1}{p_3} x + \frac{p_2}{p_3} \quad \Leftrightarrow \quad z^2 + \left(x - \frac{p_1}{2p_3}\right)^2 = \frac{4 p_2 p_3 - p_1^2}{4 p_3^2}, \tag{17}$$

where p_n are multinomials in $\mathbf{d}$ and $\mathbf{w}$ (the expressions are not given here as they are rather large). Since the properties stated in the lemma are independent of rotation, scaling, and translation it follows that it not only applies to $\widetilde{\mathcal{I}}^\triangle$, but also to $\mathcal{I}^\triangle$.

The proof for $\mathcal{I}^\circ(r)$ is equivalent. ∎

The existence of two different intersection functions for the same set of sensors might give the impression that the unknown variable r can be determined by finding the point in which the two function intersect (they have to since they both include the (x, y, z) point corresponding to $\mathbf{w}$ and $\mathbf{v}$). But as the following
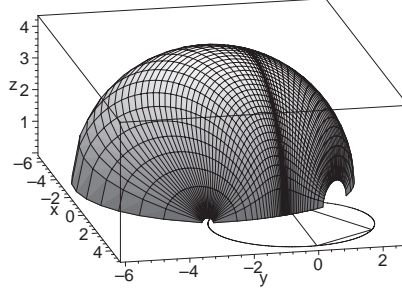
Fig. 7. The result of varying both r and w_2 subject to $r\mathbf{w} \in \mathcal{F}^\triangle_{PQS}$. All other values are from Table I and II.

lemma shows the two intersection functions provide exactly the same information. Consequently, the r cannot be determined by correlation of the two functions.

Lemma 12: Let PQS satisfy Definition 1. Let $\mathbf{w} \in \mathcal{F}^\triangle_{PQS}$ and $\mathbf{v} \in \mathcal{F}^\circ_{PQS}$ correspond to the same point in $\mathbb{R}^2 \otimes \mathbb{R}^+$. Then (i) $r\mathbf{w} \in \mathcal{F}^\triangle_{PQS}, r \in \mathbb{R}^+$ iff $r\mathbf{v} \in \mathcal{F}^\circ_{PQS}$, and (ii) $\mathcal{I}^\triangle_{PQS}(\mathbf{w}, r) = \mathcal{I}^\circ_{PQS}(\mathbf{v}, r)$ for all r where $r\mathbf{w} \in \mathcal{F}^\triangle_{PQS}$.

Proof: First (ii) is shown by substituting

$$\mathbf{w} = \frac{1}{2} \begin{bmatrix} 1 & 1 & 0 \\ 0 & 1 & 1 \\ 1 & 0 & 1 \end{bmatrix} \mathbf{v}$$

in $\mathcal{I}^\triangle_{PQS}(\mathbf{w}, r)$. Then (i) follows from Lemma 11.   ■

Since the two intersection functions are equal the notation $\mathcal{I}_{PQS}$ will be used whenever the function expression does not matter (this is usually the case in theory, and usually not the case when using real (noisy) measurements).

Finally, it is interesting to note the nice behaviour of the intersection functions when not only r, but also one of the measurements are varied. An example is shown in Fig. 7. A visual inspection might easily lead to the conclusion that if we let any two of w_1, w_2, w_3 be fixed, and vary the third, the locus given by

$$\left\{ \mathcal{I}^\triangle_{PQS}(\mathbf{w}, r) \;\middle|\; r\mathbf{w} \in \mathcal{F}^\triangle_{PQS}, r \in \mathbb{R}^+ \right\}$$

equals the intersection of $\mathbb{R}^2 \otimes \mathbb{R}^+$ and a sphere with centre in the xy plane.

While the locus is indeed close to being a half-sphere, it is not a half-sphere. However, the deviation is such that for any practical purpose, for instance denoising of measurements, the locus can be considered a half-sphere.

VII. SENSITIVITY TO NOISE

The sensitivity to noise is a key issue in any mapping of high dimensional measurement data to spatial position. It is important to have a reasonable relation between perturbations of the measurements and the

corresponding error in spatial position. In this construction the continuity of $\mathcal{I}_{PQS}$ guarantees this error to be no larger than $O\big((\Delta \mathbf{w})^2\big)$, since $\mathcal{I}_{PQS}$ contains at most second order terms of the w_n's or v_n's. However, a squaring of the error in the mapping can easily become unpleasant in an application, and is in general unacceptable.

To assess the stability of the intersection functions two simulations have been performed. In the first the three coordinates w_1, w_2, and w_3 in the measurement space has all been varied by ± 8 relative to the true value for the point F_5'. This has been done in 121 steps, such that step 1 is the true value minus 8, step 61 is the true value, and step 121 is the true value plus 8. Thus, $121^3 = 1,771,561$ measurements has been generated. The true measurement is $(13.340, 10.681, 10.905)$. For all measurements the corresponding spatial position has been determined by $\widetilde{\mathcal{I}}_{PQS}^{\triangle}$. The measurements that yields a non-real z coordinate has been removed. This amounts to $1,460,156$ of the measurements. The remaining $311,405$ measurements have been used to generated the top plot in Fig. 8. Here each measurement is plotted as a point where the first coordinate is the Euclidean distance from the measurement to the true measurement and where the second coordinate is the Euclidean distance from the corresponding spatial position to the true spatial position. The true spatial position, corresponding to the true measurement, is $(1.52, -0.690, 1.77)$. The figure does not show the points themselves, but rather a two-dimensional histogram of the points. Note that the r value used in this plot is the true value 0.295.

In the second simulation normally distributed noise with zero mean and standard deviation 2 has been applied to the true measurements. Again 121^3 measurements have been generated, and $832,509$ of these yield a real z coordinate. The bottom plot in Fig. 8 shows the result of the simulation.

This visual presentation of the relation between measurement and position error exhibits two important features. First, there is a well-behaved, approximately $O(\sqrt{\Delta \mathbf{w}})$, upper limit to the position error. This is comforting because we could not a priori expected it to be less than $O\big((\Delta \mathbf{w})^2\big)$. Second, a significant part of the measurements has an error that relates almost linearly to the position error. This means that whenever the error distribution of the of the measurements is known we have a reasonably good description of the distribution of the position error.

VIII. Combining Several Sensors

To find the location of a reflecting object it is not enough to have three sensors and an intersection function (or indeed two intersection functions based on the same set of three sensors, as demonstrated in Lemma 12). There is one unknown variable still to be determined. The r in the intersection functions cannot be determined based on reflection information from three sensors. It is therefore necessary to introduce a fourth sensor. This will result in a total of six spheroids, and any combination of three of those will give an intersection function $\mathcal{I}$. In general, for a setup with N sensors located in such a way
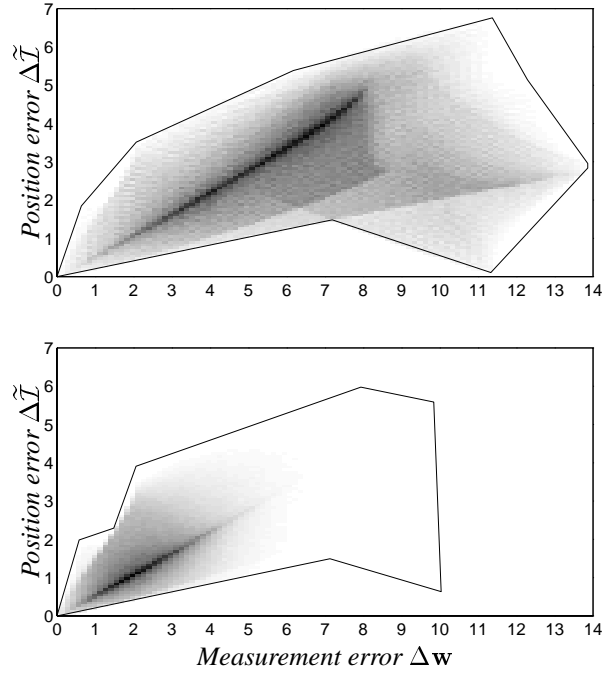
Fig. 8. A histogram of measurement error versus position error for the measurement $(13.340, 10.681, 10.905)$ corresponding to the spatial point $(1.52, -0.690, 1.77)$. The top plot shows the error for equidistant measurements, the bottom plot shows the error for normally distributed $N(0, 4)$ measurements. Dark means many points and white means no points. The scale is linear. The solid lines show boundaries outside which there are not points.

that any combination of three sensors describes a triangle there is a total of

$$\binom{N}{3} = \frac{N!}{6(N-3)!}$$

spheroid combinations. For any combination of two sensors there is a measurement and for each sensor there is further one measurement (from the sensor to the object and back to the sensor). Consequently, the total number of measurements with N sensors is

$$\binom{N}{2} + N = \frac{N!}{2(N-2)!} + N = \frac{N(N+1)}{2} \; .$$

It is obvious that in a noise-free setting four sensors provide plenty of (i.e. redundant) information for determining r. In a real life setup this redundancy can be very useful to reduce the effect of noise. A number of methods could easily be devised for this purpose (such as minimizing the mean square error), but due to limited space no method or algorithm for exploiting the redundancy is given here. However, there are some theoretical prerequisites for a stable mapping. These are related to the locations of the sensors and are discussed in the following section.

IX. LOCATIONS OF SENSORS

The multiplicity of sensors brings up a rather important question. The complete freedom in the locations of the sensors (except no three sensor can be on a line) makes it relevant to ask what the optimal locations are for N sensors. This question relates to real applications, since the task of finding the location of the reflecting object is trivial (once the intersection function is given) in a theoretical setting. Optimality of sensor locations in this context means locating the sensor such as to have the determination of the location of the reflecting object being least sensitive to factors such as measurement noise, hardware degeneration, finite accuracy, rounding errors etc. which inevitably will affect the quality of the conversion from high dimensional data to three dimensions. Finding the optimal sensor locations thus becomes a matter of combining the influence of each of these factors with the behaviour of the intersection function. Note that the four sensors in Fig. 3 are not in any way claimed to be optimally located, they are merely located in what seems to be a nice and close-to-symmetric way.

Although optimality to a large extent depends on a priori unknown factors there are still some theoretical consideration worth doing. In fact, some choices of sensor locations leads to an inherently unstable mapping. For the purpose of considering theoretical optimality the first step is to determine which mathematical properties of the intersection functions have any influence in this context, and the second step is to determine which model parameters governs these properties.

A. Optimal Locations

The location of the reflecting object is found as the common point of the intersection curves described in the previous sections. Without noise this point is uniquely defined since all intersection curves coincide at the same point. With noise chances are that no two intersection curves coincide. In the latter case some method is needed to determine which point is 'best' or 'closer' to the right point. This method is necessarily based on not just a single point on each intersection curve, but rather on a interval of the curve, or indeed the whole curve. With two intersection curves a possible solution is to determine the smallest distance between (points on) the two curves, and then let the 'intersection point' be the point which is located half way in between. The question of usefulness of this particular approach is left unanswered at this point. It is easy to come up with variations on this idea, and they all share the need for finding some distance between two (or more) curves. Such an operation is less sensitive when the curves are closer to being perpendicular than parallel. The primary question is therefore (in regards to sensor locations) how to control the intersection curves such as to comply with the desire to have 'mostly perpendicular curves'.

This is to some extent easily answered by Lemma 11 which states that any intersection curve projected onto the xy plane is part of a line going through the centre of the circumscribed circle. Thus, having the

centres well separated guarantees a not insignificant angular difference between the curves. Moreover, the curves exist in three dimensions, a fact that can cause an increase, but never decrease, in the angular difference.

This raises two new question: 1) What is the optimal location of the centres, and 2) how can the centres be placed in a given pattern? The latter question is relevant since the locations of the centres are completely determined by the location of the sensors.

There are one important observation relating to the first question. Whenever the (x, y) coordinate of the common point of the intersection curves (i.e. the projection of the position of the reflecting object onto the xy plane) lies within the convex hull spanned by the centres of the circumscribed circles (which is a quadrilateral with four sensors) there is a lower limit determined by the 'flatness' of the convex hull to the angles between the intersection curves. No such limit exists outside this convex hull. This lower limit is relatively high when the 'flatness' of the convex hull is small. For a four sensor setup this observation is in favor of a large, close to being square, quadrilateral.

But the two questions cannot be finally answered independently, especially not in a real setup which is subject to physical constraints. The dependency between the location of sensors (or more accurately, corners of the triangles) and the centres of the circumscribed circles is by no means linear in behaviour, and consequently small adjustments of the location of a corner might have a significant effect on the location of the centre, and vice versa. Moreover, some pattern of centres cannot be achieved (except in a limit sense).

One choice of sensor locations is easily recognized as being poor; if the sensors are located such that they span a square all four centres of the circumscribed circles coincide, and in which case all four intersections functions also coincide. This in turn leads to a degenerate solutions set, i.e. it is not possible to determine the r based on this sensor setup.

B. Sensor Locations and Centres of Circumscribed Circles

It is fairly easy to describe the relation between four sensors and the centres of the circumscribed circles. Since the centre of the circumscribed circle to a triangle is the intersection point of the three perpendicular bisectors of the sides, each of the four centres is found as the intersection point of the perpendicular bisectors of two adjacent sides in the (non-intersecting) quadrilateral spanned by the four sensors. This is shown in Fig. 9 where the sensor locations are named (x_n, y_n) and the centres are named $(\tilde{x}_n, \tilde{y}_n)$.

Two things are immediately noted. First, the quadrilateral spanned by $(\tilde{x}_n, \tilde{y}_n)$ looks like it might be congruent to the quadrilateral spanned by (x_n, y_n). Second, the two points $(\tilde{x}_1, \tilde{y}_1)$ and $(\tilde{x}_2, \tilde{y}_2)$ lie on the perpendicular bisector to the side $(x_1, y_1) - (x_2, y_2)$ (and likewise for the three other sides).
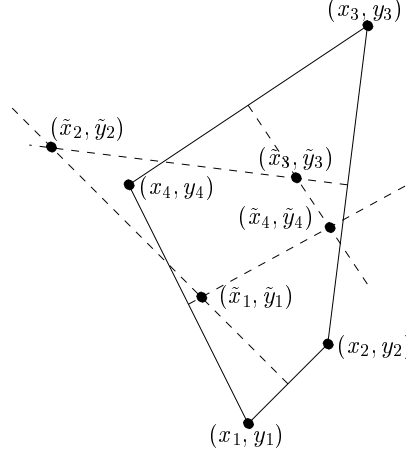
Fig. 9. Four sensors span a quadrilateral (solid line) and a total of four circumscribed circles can be generated. The four centres each lies on the two perpendicular bisectors (dashed lines) of the sides which are shared by the quadrilateral and the circumscribed triangle.

The first observation is unfortunately not correct. To each angle v_n in the original quadrilateral there is a corresponding angle ν_n such that $\nu_n = \pi - v_n$. Although this gives a close relation between the two quadrilaterals, it means that they are not in general congruent. They are in special cases, for instance when two opposing sides are parallel. The relation between the two quadrilaterals can be uniquely determined, however. Incidentally, the second observation provides the equations necessary to derive this relation.

Since the line $\tilde{\ell}$ through $(\tilde{x}_1, \tilde{y}_1)$ and $(\tilde{x}_2, \tilde{y}_2)$ is perpendicular to the line ℓ through (x_1, y_1) and (x_2, y_2) we have

$$
\begin{bmatrix} x_1 - x_2 & y_1 - y_2 \end{bmatrix} \begin{bmatrix} \tilde{x}_1 - \tilde{x}_2 \\ \tilde{y}_1 - \tilde{y}_2 \end{bmatrix} = 0 \ ,
\tag{18}
$$

and likewise for the three other sides. We also note that $\tilde{\ell}$ intersects ℓ at the midpoint between (x_1, y_1) and (x_2, y_2). Since the inner product of the normal vector to a line and any point on the line is the same for all points, we also have

$$
\begin{bmatrix} \tilde{y}_2 - \tilde{y}_1 & \tilde{x}_1 - \tilde{x}_2 \end{bmatrix} \begin{bmatrix} x_1 + x_2 \\ y_1 + y_2 \end{bmatrix} = 2 \begin{bmatrix} \tilde{y}_2 - \tilde{y}_1 & \tilde{x}_1 - \tilde{x}_2 \end{bmatrix} \begin{bmatrix} \tilde{x}_1 \\ \tilde{y}_1 \end{bmatrix} ,
\tag{19}
$$

and likewise for the three other sides. It is possible to find other equations describing the relations, but the ones presented here have one nice property; they are linear in the unknowns (x_1, y_1) through (x_4, y_4).

Expanding the eight equations gives the following equation to be solved

$$
\begin{bmatrix}
\tilde{x}_1-\tilde{x}_2 & \tilde{y}_1-\tilde{y}_2 & \tilde{x}_2-\tilde{x}_1 & \tilde{y}_2-\tilde{y}_1 & 0 & 0 & 0 & 0 \\
0 & 0 & \tilde{x}_2-\tilde{x}_3 & \tilde{y}_2-\tilde{y}_3 & \tilde{x}_3-\tilde{x}_2 & \tilde{y}_3-\tilde{y}_2 & 0 & 0 \\
0 & 0 & 0 & 0 & \tilde{x}_3-\tilde{x}_4 & \tilde{y}_3-\tilde{y}_4 & \tilde{x}_4-\tilde{x}_3 & \tilde{y}_4-\tilde{y}_3 \\
\tilde{x}_1-\tilde{x}_4 & \tilde{y}_1-\tilde{y}_4 & 0 & 0 & 0 & 0 & \tilde{x}_4-\tilde{x}_1 & \tilde{y}_4-\tilde{y}_1 \\
\tilde{y}_1-\tilde{y}_2 & \tilde{x}_2-\tilde{x}_1 & \tilde{y}_1-\tilde{y}_2 & \tilde{x}_2-\tilde{x}_1 & 0 & 0 & 0 & 0 \\
0 & 0 & \tilde{y}_2-\tilde{y}_3 & \tilde{x}_3-\tilde{x}_2 & \tilde{y}_2-\tilde{y}_3 & \tilde{x}_3-\tilde{x}_2 & 0 & 0 \\
0 & 0 & 0 & 0 & \tilde{y}_3-\tilde{y}_4 & \tilde{x}_4-\tilde{x}_3 & \tilde{y}_3-\tilde{y}_4 & \tilde{x}_4-\tilde{x}_3 \\
\tilde{y}_4-\tilde{y}_1 & \tilde{x}_1-\tilde{x}_4 & 0 & 0 & 0 & 0 & \tilde{y}_4-\tilde{y}_1 & \tilde{x}_1-\tilde{x}_4
\end{bmatrix}
\begin{bmatrix}
x_1 \\ y_1 \\ x_2 \\ y_2 \\ x_3 \\ y_3 \\ x_4 \\ y_4
\end{bmatrix}
= 2
\begin{bmatrix}
0 \\ 0 \\ 0 \\ 0 \\
\tilde{y}_1\tilde{x}_2 - \tilde{x}_1\tilde{y}_2 \\
\tilde{y}_2\tilde{x}_3 - \tilde{x}_2\tilde{y}_3 \\
\tilde{y}_3\tilde{x}_4 - \tilde{x}_3\tilde{y}_4 \\
\tilde{y}_4\tilde{x}_1 - \tilde{x}_4\tilde{y}_1
\end{bmatrix}.
\tag{20}
$$

Note that the first row corresponds to (18), while the fifth row corresponds to (19). Solving this equation means inverting the square matrix. Fortunately, the matrix has full rank in most cases. Examples of degenerate cases are when the two center points coinciding and when the four centres span a rectangle (in both cases the rank is 6). Assuming that the matrix is not degenerate the solution to (20) is provided directly by inverting the matrix. This yields a set of solutions which are all rational functions with second order multinomials in numerator and denominator. Each of the eight solution expressions are quite large, and therefore not printed here.

While these solution expressions do not by themselves provide much knowledge on the relation between the location of sensors and the centres of the circumscribed circles, they do provide easy means for numerical experiments regarding sensor and centre locations.

C. Examples of Sensor Locations

An important conclusion of the results presented in the previous section is that locating the sensors in a rectangle (or close to a rectangle) is a bad idea in respect to robustness. The sensor locations in Fig. 3 are no exception, as Fig. 10 shows. Here the four centres of the circumscribed circles are shown along with the intersection curves for the point $(4, 3.5, 2)$. It is immediately evident from the figure that determining the position of the reflecting object is very sensitive to variations in the intersection curves because they are almost parallel. Moving one sensor to another location (here F_2 are moved from $(9, 5)$ to $(9, 1)$) improves the robustness even though the quadrilateral spanned in the latter case seems to be just as close to a rectangle as the quadrilateral in the former case.

It is important to note that the sensitivity is high in the first example independently of the location of the reflecting object since the centres of the circumscribed circle almost coincide. In the second example the sensitivity is reduced because the directions to the four centres are more different. It is therefore an important observation that the centres now span a significantly larger quadrilateral. Choosing a completely
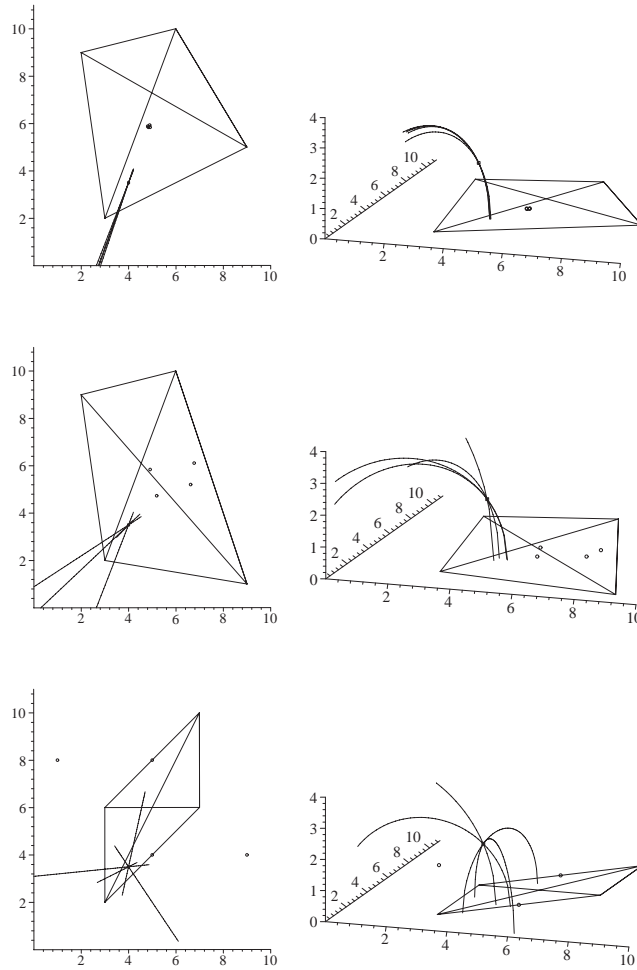
Fig. 10.   Three different locations of sensor. The solid lines show the quadrilateral and triangles spanned by the sensors, while the four small circles shown the centres of the circumscribed circles. The left column shows the projection onto the xy plane.

different set of locations, see the third examples in Fig. 10, can give a much higher robustness since the quadrilateral spanned by the centres is significantly larger than in the second examples.

X. Assumptions Revisited

There are a number of differences between the presented model and reality. The most obvious and important ones were presented in Section IV. They are still valid and they do raise the question on the usability of the model. Being clearly inaccurate the model does not provide the final solution to the mapping from high dimensional data to 3D position, and the usability is therefore more of a qualitatively kind rather than quantitatively. This section briefly discusses the importance of the model inaccuracy, possible ways of handling this, and what effect they have on the solution given by the model.
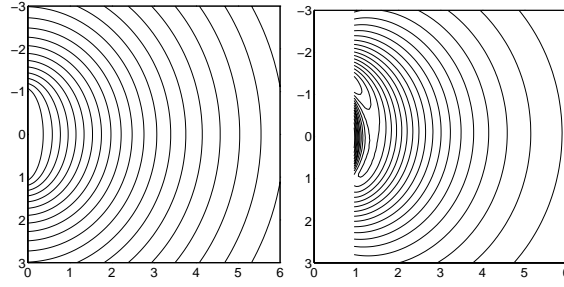
Fig. 11. Iso-intensity curves for (left) the simple model (1) and (right) for a much more complex model, here with a reflecting disc with radius 1. The latter is quite accurate, see la Cour-Harbo [10]. The emitter and receiver are located in $(0, -1)$ and $(0, 1)$, respectively.

A. Emitter and Receiver Characteristics

The choice of ellipses (and thus spheroids) to model the reflection map in Section V were primarily based on two assumptions. The first was that the emitters and receivers have uniform directional characteristics, the second was that the reflecting object has an ability to reflect light in a certain manner. The former assumption is discussed here, while the second assumption is discussed in the next subsection.

In order to give a qualitative description of the significance of the directional characteristics of the emitters and receivers Fig. 11 shows the contours of the reflection map resulting from the simple model, and contours in a reflection map generated by a quite accurate modeling of the emitter/receivers setup, see la Cour-Harbo [10]. While the former assumes uniform directional characteristics, the latter assumes characteristics on the form $a \cos(\theta)$ (the actual values of a is based on infra red emitter and receiver diodes). This model also includes a modeled surface reflection and spatial extension of the components. Although this model reveals an asymmetric behaviour it is reasonably close to the simple form used here for constructing the geometrical solution. Although the difference is too big to be neglected it seems fair to assume that the qualitative conclusions drawn here does to some extent apply to real setups, too.

B. The Reflecting Object

The basic assumption on the reflection object is that it should reflect the light such that the resulting iso-intensity sets are prolate spheroids. This was a consequence of the model in (1). This calls for a specular reflection in the direction of the receiver. The former property is easily achieved, whereas the second posses a problem. As it was hinted it is not possible to have reflections in different directions in the same point. A very small sphere comes close, but does not obtain the exact property except in a limit sense. Using a very small sphere might therefore be a good idea, at least in a theoretical setting where the emitter is considered a point source. In a real setting where the emitter has a finite spatial extension
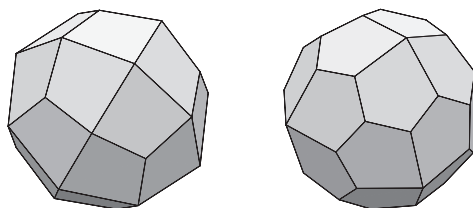
Fig. 12. A trapezoidal (left) and a pentagonal (right) icositetrahedron.
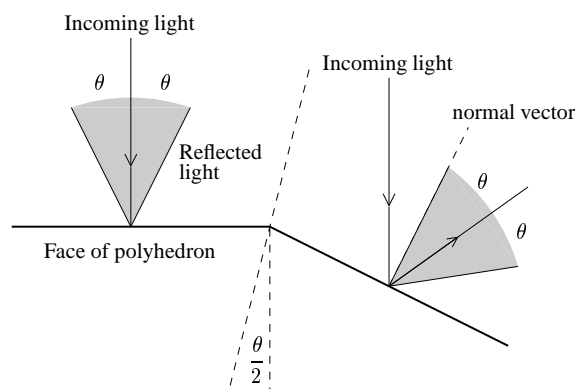

Fig. 13. The principle for an alternative reflecting object.

the curvature of the reflecting object determines the amount of light reflected in any given direction, in particular towards the receiver, i.e. the smaller the sphere, the smaller the reflection of the emitter looks from the receiver's point of view. Enlarging the sphere does reduce this problem, but at the same time the object becomes more distant from the property of reflecting in different directions from the same point in space.

Perhaps a satisfactory object, i.e. a good trade-off between the opposing desired properties, can be constructed in the following way. The object is constructed using a convex polyhedron with a sufficient high number of faces and with (almost) equal angles between them. This could be for instance a trapezoidal or pentagonal icositetrahedron (24 faced polyhedron). The faces must have a slight diffuse reflection such that in the case where a face of the polyhedron is almost, but no quite tangent to a spheroid, there is still some light reflected onto the receiver. More precisely, the reflection characteristic of the surface should be such that an incoming ray of light perpendicular to the surface is reflected such that the outgoing rays of light covers a range from $[-\theta; \theta]$, where angle 0 is perpendicular to the surface and where θ is the angle between normal vectors to two adjacent faces on the polyhedron. The principle is shown in Fig. 13. As this figure demonstrates the object will have the property that any two faces will reflect the incoming light in a way that forms disjoint cones of reflected light. Each cone represents an angle equal to the angle between normal vectors of adjacent faces. This will enable the object to reflect light in all direction

(like a sphere) without the incoming light being reflected in any direction by more than one face. Such an object would indeed be tangent to several different spheroids at almost the same point (provided that the object is small), while at the same time taking into account the finite size of the emitter. The downside is the introduction the diffuse reflection. However, the need for this this is kept at a minimum by the many-faced polyhedron.

XI. CONCLUSION

A geometrical model of the mapping of measured reflected intensities to spatial position has been presented. A series of assumptions were imposed to reduce the complexity of the model, and a number of parameters were included to provide a flexible model. The result is a mapping which in some respects is quite useful for determining properties of multiple emitter/receiver setups, but in other respects is inaccurate to an extent which rules out the immediate use in real applications. Despite the fact that the model is quite restricted by the assumptions the model is still rather complex. Though, not to a degree which prohibits implementation in signal processing hardware.

The result of modeling the multiple emitter/receiver setup is a set of equations which directly maps measurements to a coordinate in $\mathbb{R}^3$. The geometrical derivation ensures the analytical correctness of the equations, but does not guarantee numerical stability. On the contrary, the equations includes second order polynomial forms which typically have a inherent instability problem. But is was demonstrated that, at least for a specific case, the mapping exhibits a reasonable degree of stability.

The question of the optimal locations of the emitters and receivers was also discussed. An analysis of the mapping equations revealed that certain sensor positions were a priori bad in the sense that the mapping becomes very sensitive to disturbances independently of any stabilizing methods applied to the data (such as filtering). In fact, it was demonstrated that placing emitter and receivers at the corners of a square increased the sensitivity to infinite as a singularity in the mapping occurs in that situation. It was also discovered that a best case scenario is application specific as the optimal placement depends on the space available for arranging the emitters and receivers.

REFERENCES

[1] T. Rindfleisch, "Photometric method for lunar topography," *Photogrammetric Engineering*, vol. 32, no. 2, pp. 262 – 277, 1966.

[2] B.K.P. Horn, "Understanding image intensities," *Artificial Intelligence*, vol. 8, no. 2, pp. 201 – 231, April 1977.

[3] B.K.P. Horn, "Height and gradient from shading," *International Journal of Computer Vision*, vol. 5, no. 1, pp. 37 – 75, August 1990.

[4] A. Pentland, "The transform method for shape-from-shading," Tech. Rep. 106, MIT Media Lab Vision Sciences, July 15 1988.

[5] B.V.H. Saxberg, *A Modern Differential Geometric Approach to Shape from Shading*, Ph.D. thesis, Department of Electrical Engineering and Computer Science,MIT, Cambridge,MA., 1988.

[6] A. la Cour-Harbo and J. Stoustrup, "Using spread spectrum transform for fast and robust simultaneous measurement in active sensors with multiple emitters," in *Proceedings of IECON '02*. IEEE, September 2002, pp. 2669 – 2674, IEEE Catalog 02CH37363, ISBN: 0-7803-7474-6.

[7] A.J. Viterbi, *CDMA: Principles of Spread Spectrum Communications*, Addison-Wesley, Reading, MA, 1995.

[8] E. Biglieri, D. Divsalar, P.J. Mclane, and M.K. Simon, *Introduction to Trellis-Coded Modulation with Applications*, Macmillan Publishing Company, 1 edition, 1991.

[9] A. F. Molisch, *Wideband Wireless Digital Communications*, Prentice Hall, 2000, ISBN: 0-13-022333-6.

[10] A. la Cour-Harbo, *Robust and Low-Cost Active Sensor by means of Signal Processing Algorithms*, Ph.D. thesis, Aalborg University, Dept. of Control Engineering, Fredrik Bajers Vej 7C, DK-9220 Aalborg East, Denmark, August 2002.
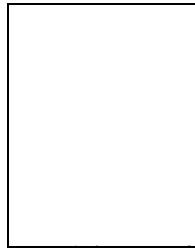
Anders la Cour-Harbo was born on December 26th, 1973, in Denmark. He received the Bachelor degree in mathematics in 1996, and Master degree in mathematics and digital signal processing in 1998, both from Aalborg University, Denmark. He received his Ph.D. in August 2002. Currently assistant professor at Department of Control Engineering, Aalborg University. He has spent six month at Royal Institute of Technology, Stockholm, Sweden as Visiting Researcher. Co-founded in November 1999 BeamControl ApS, and co-author on 'Ripples in Mathematics - The Discrete Wavelet Transform', Springer 2001. His research interests focus on the area of combining mathematics and electronic engineering, in particular in low-cost sensor systems.